Control of Lay on Cobalt Chromium Alloy Finished Surfaces Using Magnetic Abrasive Finishing and Its Effect on Wettability

Arthur A. Graziano
Department of Mechanical and Aerospace Engineering, University of Florida, Gainesville, FL 32611

Vasishta Ganguly
Department of Mechanical Engineering and Engineering Science, University of North Carolina at Charlotte, Charlotte, NC 28223

Tony Schmitz
Department of Mechanical Engineering and Engineering Science, University of North Carolina at Charlotte, Charlotte, NC 28223

Hitomi Yamaguchi
Department of Mechanical and Aerospace Engineering, University of Florida, Gainesville, FL 32611

Freeform surfaces, including the femoral components of knee prosthetics, present a significant challenge in manufacturing. The finishing process is often performed manually, which leads to surface finish variations. In the case of knee prosthetics, this can be a factor leading to accelerated wear of the polyethylene tibial component. The wear resistance of polyethylene components might be influenced by not only the roughness but also the lay of femoral component surfaces. This study applies magnetic abrasive finishing (MAF) for nanometer-scale finishing of cobalt chromium alloys, which are commonly used in knee prosthetics and other freeform components. Using flat disks as workpieces, this paper shows the dominant parameters for controlling the lay in MAF and demonstrates the feasibility of MAF to alter the lay while controlling the surface roughness. The manually finished disk surfaces (with roughness around 3 nm S_a*), consisting of random cutting marks, were compared to MAF-produced surfaces (also with roughness around 3 nm* S_a*) with different lays. Tests using deionized water droplets show that the lay influences the wetting properties even if the surface roughness changes by no more than a nanometer. Surfaces with unidirectional cutting marks exhibit the least wettability, and increasing the cross-hatch angle in the MAF-produced surfaces increases the wettability. Surfaces consisting of short, intermittent cutting marks were the most wettable by deionized water.*
[DOI: 10.1115/1.4026935]

1 Introduction

Freeform surfaces present a great deal of difficulty in the manufacturing process. For example, the geometry of artificial knee joint surfaces is produced by grinding, and a finishing process is required following grinding to reduce the surface roughness to less than 5 nm S_a without disturbing the form accuracy. Freeform finishing in practical use (e.g., in optical-related industries) has been reportedly automated using two technologies using flexible tools: magnetorheological (MR) fluid polishing [1–4] and bonnet polishing [5–7]. The former process uses MR polishing fluid as a polishing tool. The rheological properties (e.g., viscosity) can be controlled by a magnetic field. The behavior of the fluid suspended in a magnetic field enables it to form a tool to polish while conforming to a freeform surface. The latter process uses a reinforced rubber tool attached to a seven-axis computer numerically controlled (CNC) machine tool. Physical contact of the tool against a freeform surface causes the tool to deform and conform to the workpiece. Both of these flexible tools have been applied to the surface finishing of the femoral components of knee prosthetics [8–10]. Although these and other laboratory-level technologies are ever progressing, to improve the surface quality by orders of magnitude, a significant advance is highly desired. Moreover, the surface finishing of freeform surfaces is often performed manually in practice, increasing quality variation and production costs. The surface irregularities of the femoral component cause wear of the ultrahigh molecular weight polyethylene (UHMWPE) tibial component as the two components rub against one another and create debris. This is often cited as the primary cause of tissue inflammation and osteolysis leading to a wide range of medical issues including eventual failure [11,12].

Tribological studies of UHMWPE and stainless steel couplings have found that the wear factor increases exponentially with increasing surface roughness [11]. The wear rate may be enhanced—and thus the longevity of prosthetics—by decreasing the surface roughness. Additionally, material wettability has also been shown to play a role in wear [13]. Research shows that contact between two solid surfaces that have a large difference in wettability leads to an increased fluid film thickness between the surfaces, which results in a reduced wear rate [13]. Specifically, research shows that in order to increase the fluid film thickness, the pin in pin-on-disk experiments must display hydrophilic properties while the disk must display hydrophobic properties [14]. Observing that the bearing surface on a knee prosthetic consists of a relatively flat UHMWPE tibial component and a freeform curved femoral part, the authors hypothesize that the wear rate in the prosthetic would decrease with the combination of a more hydrophilic femoral component and a less hydrophilic tibial component.

It is known that surface roughness has a significant correlation with contact angle (a measure of surface wettability) [15–17]; this trend has been exploited to improve component performance in various fields, such as in the biomedical, chemical, electrical, and mechanical fields [18–21]. In addition to surface roughness, surface lay (repetitive impressions created on the surface of a part) is considered to be a critical factor affecting the fluid film condition between solid bodies and the coefficient of sliding friction for precision finished surfaces [22,23]. In a study on the honing of engine cylinder liners, cross-hatch angles and groove patterns on the liner surfaces were shown to play important roles in the sliding friction of components and thus engine performance [24]. Although the focuses of these previous studies were on the submicron to

Contributed by the Manufacturing Engineering Division of ASME for publication in the Journal of Manufacturing Science and Engineering. Manuscript received November 30, 2012; final manuscript received February 18, 2014; published online April 11, 2014. Assoc. Editor: Allen Y. Yi.

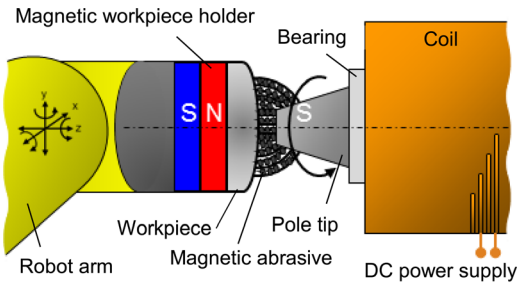

(a) Processing principle

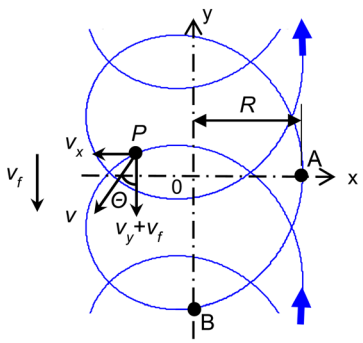

(b) Resultant particle motion

Fig. 1 MAF processing principle

micrometer scales, similar effects might be shown on the nanometer scale. In other words, controlling surface texture and the surface roughness on the nanometer scale might show potential for increasing the hydrophilicity of femoral components, thereby improving the wear resistance of tibial components in knee prosthetics.

MAF has been used to finish freeform surfaces and other complex geometries because of its characteristics including flexible magnetic particle chains that form along the lines of magnetic force and conform to the workpiece surface [25–27]. The material removal mechanism of MAF is attributed to microcutting of the surface, and the motion of the magnetic particle tools results in characteristic surface textures [28–30]. Accordingly, this study proposes the application of MAF to finish cobalt chromium (CoCr) alloy components and modify their surface texture. The finishing equipment was specifically designed and built for this study, and flat disks are used as workpieces. This paper studies the dominant parameters for controlling the lay with MAF and demonstrates the feasibility of MAF to alter the lay while controlling the surface roughness. Using four different surface lays produced by MAF, the effects of lay on the contact angle of deionized water (i.e., the wettability) are studied.

2 Processing Principle

A schematic of the principle for finishing freeform surfaces is shown in Fig. 1. In this MAF process, material is removed by an abrasive slurry pushed by magnetic particles in the presence of a magnetic field. The CoCr alloy workpiece is nonmagnetic, so the workpiece is mounted on a magnetic workpiece holder to generate the magnetic circuit needed to form magnetic particle chains between the north (N) and south (S) poles normal to the target surface. The magnetic force acting on the particle F is given by

$$F = V\chi H \cdot \nabla H \tag{1}$$

where V is the volume of the magnetic particle, χ is the magnetic susceptibility, and H and ∇H are the intensity and gradient of the magnetic field at the finishing area, respectively [31].

The abrasive slurry is introduced between the target surface and magnetic particles, and only the abrasives pushed by the magnetic particles (with the force shown by Eq. (1)) perform the finishing action. When the pole tip rotates, the mixture of magnetic particles and abrasive slurry rotates with the pole tip, generating relative motion between the abrasive slurry and target surface. The feed motion of the workpiece extends the finishing area to cover the entire surface of the freeform component.

If the workpiece is fed linearly in the vertical direction, the pole-tip rotation and the workpiece feed combine to drive the abrasive along the path shown in Fig. 1(*b*). The cutting velocity v and inclination angle Θ at any point P is calculated using the following equations:

$$\mathrm{v} = \sqrt{(-\mathrm{r}\omega \sin\ \omega\mathrm{t})^2 + (\mathrm{r}\omega \cos\ \omega\mathrm{t} + \mathrm{v_f})^2} \tag{2}$$

$$\Theta = \tan^{-1}(-\mathrm{r}\omega \sin \omega\mathrm{t}/(\mathrm{r}\omega\ \cos\ \omega\mathrm{t} + \mathrm{v_f})) \tag{3}$$

where v_f is the workpiece feed velocity, r is the distance from the pole-tip center to the particle, ω is the angular velocity, and t is the finishing time. Both Eqs. (2) and (3) are a function of finishing time, t.

The magnetic particles are suspended along the lines of magnetic force, and the particles suspended at the edge of the pole tip ($r = R$) show the highest cutting velocity. The cutting velocity v is maximum (v_{max}) at position A (as shown in Fig. 1(*b*)) and calculated as

$$\mathrm{v_{max}} = \mathrm{v_f} + \mathrm{R}\omega \tag{4}$$

In a strong mangetic field, the magnetic particles form stiff chains. The particle chains and abrasive slurry rotate with the pole tip and show continuous relative motion against the target surface to create a surface finished with long cutting marks [29]. By modifying the workpiece feed v_f and angular velocity ω, the instantaneous cutting velocity v and inclination angle Θ are altered, resulting in different lays on the finished surface. If the magnetic force is reduced, the magnetic particles may not rotate with the pole tip; instead, they may relocate (change position) within the particle chains and may release the abrasive slurry as a result of friction against the workpiece surface. In turn, the finished surface is an accumulation of short, intermittent cutting marks. In the internal finishing of nonmagnetic tubes, a similar trend has been observed when using slurry with iron particles several micrometers in diameter [30]. When the magnetic force is even weaker, the magnetic particles are spun off and no finishing occurs.

3 Finishing Machine

The experimental setup shown in Fig. 2 was developed to materialize the described principle. It consists of a magnetic field generator and a workpiece holder attached to a six-axis robot. The magnetic workpiece holder and nonmagnetic jig (Fig. 2(*b*))are made of 1018 carbon steel and 6061 aluminum, respectively. The magnetic component creates a magnetic circuit so that the finishing area (workpiece surface) is in the magnetic field as required for finishing. The nonmagnetic jig separates the robot electronics from the magnetic field. The workpiece holder shown is designed for the flat discs (Ø31.8 × 6.3 mm) used in this study.

The coil shown in Fig. 2(*a*) was fabricated by winding 4230 turns of 18 AWG (Ø1.024 mm) insulated copper wire around a double-layered insulated core (Ø40 × 145 mm) made of 1144 carbon steel. The total resistance of the coil is 22.84 Ω. The coil is connected to a dc power supply, and the exciting current can be varied up to 2.63 A. As shown in Fig. 2(*c*), one end of the coil has a spindle attached to an interchangeable pole tip, which is rotated by a motor-driven pulley. To vary the magnetic field at the finishing area, this pole tip can be changed in addition to changing the exciting current.

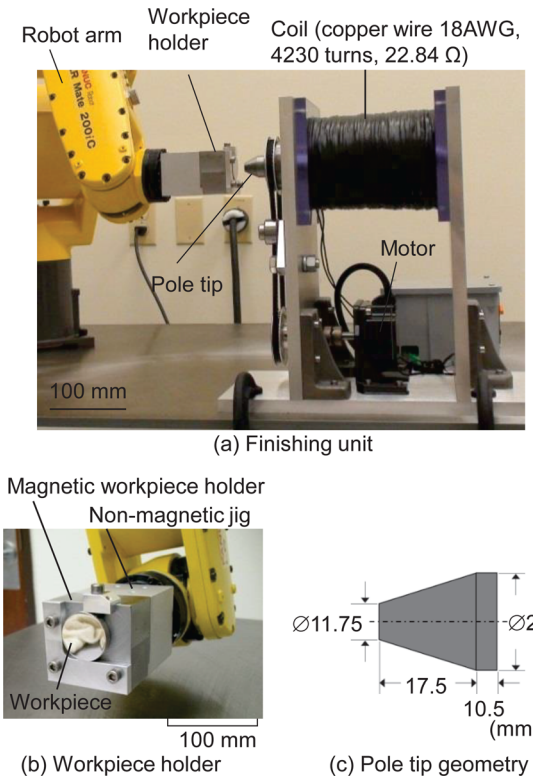

Fig. 2 Photograph of experimental setup and pole-tip geometry

4 Finishing Conditions and Experimental Protocol

CoCr alloy disks were used as workpieces in this study (the geometry is shown in Fig. 3(*a*)). To analyze the changes in surface roughness and lay, the surface was evaluated at five areas using an optical surface profilometer with a lateral resolution of 275.7 nm and a vertical resolution of < 0.1 nm. A 150 μm $\times$ 100 μm target area at each location was filtered using a Gaussian spline band pass filter with low and high cutoff wavelengths of 30 μm and 0.828 μm, respectively. Figure 3(*b*) shows an image obtained from the optical profilometer of the as-received surface (taken at location L3), which demonstrates the typical characteristics of the manually finished surface. It is composed of multidirectional scratches of various lengths with occasional very deep scratches. Although the surface roughness value varies by measurement location, the as-received roughness was typically around 3 nm S_a.

Since one of the goals of this study was to find the relationship between surface lay and wettability, the challenge was to set conditions that altered the lay with minimal changes to the roughness S_a. This study uses control of the magnetic force acting on the magnetic particles (dependent on particle volume and exciting current), workpiece feed rate, and pole-tip revolution rate to produce four different surface lays. The finishing conditions are provided in Table 1, and the parameters were chosen based on prior experimental finishing results [32]. Iron particles with two different size distributions, 0–45 μm and 45–150 μm, were used. The workpiece feed rates were 1, 10, and 50 mm/s. The rates of pole-tip revolution were 100, 150, or 500 min^{-1}. The combinations applied are listed in Table 1.

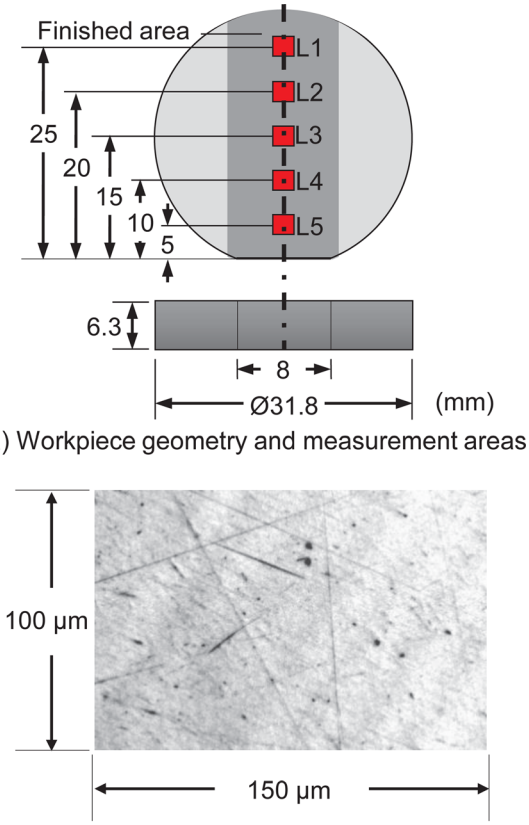

Fig. 3 Workpiece geometry, roughness measurement areas, and optical image of as-received surface

Figure 4 shows the particle paths in conditions 1, 2, and 3. The value of Θ at position B (as shown in Fig. 1(*b*)) in conditions 1, 2, and 3 was calculated using the following equation to be 50.9 deg, 80.8 deg, and 89.8 deg, respectively:

$$\Theta_B = \tan^{-1}(-R\omega/v_f) \quad (5)$$

Table 1 Finishing conditions

				4	
Condition	1	2	3	a	b
Diamond abrasive size, μm	0–0.25	0–0.25	0–0.5	0–0.25	
Diamond abrasive amount, mg			50		
Iron particle size, μm		45–150		0–45	
Iron particle amount, mg		500		500	300
Workpiece feed rate, mm/s	50	10	1	1	
Workpiece feed, mm			43		
Pole-tip revolution, min^{-1}	100	100	500	500	150
Pole tip–workpiece distance, mm			1		
Exciting current, A		2.5		2.5	1.0
Magnetic flux density at center of pole tip, T		0.23		0.23	0.13
Finishing time, min		15		15	45

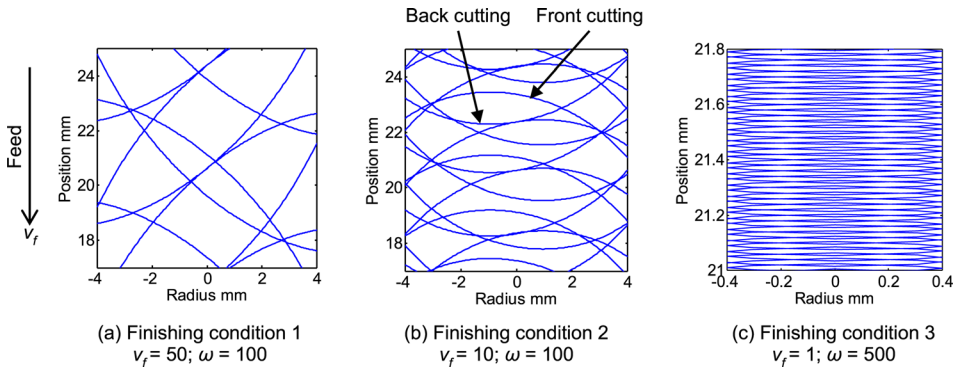

Fig. 4 Schematic of cutting marks for finishing conditions 1, 2, and 3

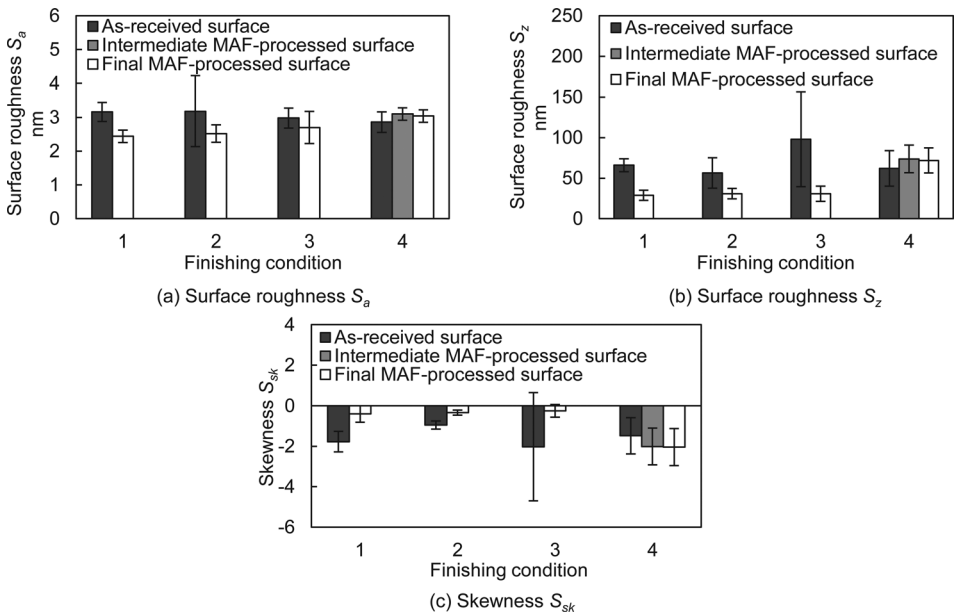

Fig. 5 Relationship between surface roughness, skewness, and finishing conditions

Two-phase finishing was applied in condition 4, which was designed to produce short, intermittent cutting marks. The first phase produced the desired lay but with a slightly increased roughness. The second phase reduced the roughness S_a without disturbing the surface lay.

The finishing experiments started from the center of the workpiece, and the workpiece was fed up and down (total finished length: 43 mm) while the pole tip rotated. This up-and-down motion was repeated for the duration of the finishing trial. After the completion of the finishing trials, the workpiece was cleaned by rinsing it with deionized water and ethanol, followed by drag wiping with a single-use cotton wipe, and finally rinsing with acetone.

5 Finishing Characteristics

Finishing experiments for each condition were conducted twice; representative results from each finishing experiment are reported in this paper. Figure 5 shows changes in average surface roughness S_a, peak-to-valley height S_z, and skewness S_{sk} at locations L1–L5 for each finishing condition. The values reported are averages of the measurements at each location (error bars correspond to $\pm$ one standard deviation, 1σ). Conditions 1–3 show improvement in the surface roughness after MAF. Condition 4 a shows a slightly increased surface roughness, and condition 4 b only slightly reduced the roughness from condition 4 a. The skewness in conditions 1–3 increased toward zero. In condition 4, the material removal was considerably low and the deep scratches that were originally present still remain after finishing. The result is almost no change in S_a, S_z, or S_{sk} regardless of the changes in the surface lay. However, after the deep scratches were excluded from the $100\,\mu m \times 150\,\mu m$ area, S_a was 3 ± 0.2 nm, S_z was 30 ± 9 nm, and S_{sk} was -0.7 ± 0.2 in a $100\,\mu m \times 60\,\mu m$ area; these values are similar to those obtained in conditions 1–3. Overall, Fig. 5 suggests that the conditions used in this study more uniformly finished the target surface with minimal influences in the roughness parameters S_a and S_z and skewness S_{sk}.

Figure 6 shows optical images of finished surfaces. These images demonstrate the effects of finishing conditions on the surface lay. In conditions 1–3, irregular, multidirectional scratches, and dents on the as-received surfaces (Fig. 3(*b*)) have been removed by MAF. The lays resulted from long cutting marks that were generated by the abrasives pushed by the large magnetic particles. The angle ϕ (the *cross-hatch angle*) shown in Figs. 6(*a*) and 6(*b*) was measured for conditions 1–3. Five locations on the optical images of the finished surfaces (shown in Fig. 6) were chosen for the angle measurements. Using ten optical images of each condition, the angles from fifty locations were measured, and the averages of the fifty values were reported as the cross-hatch angle

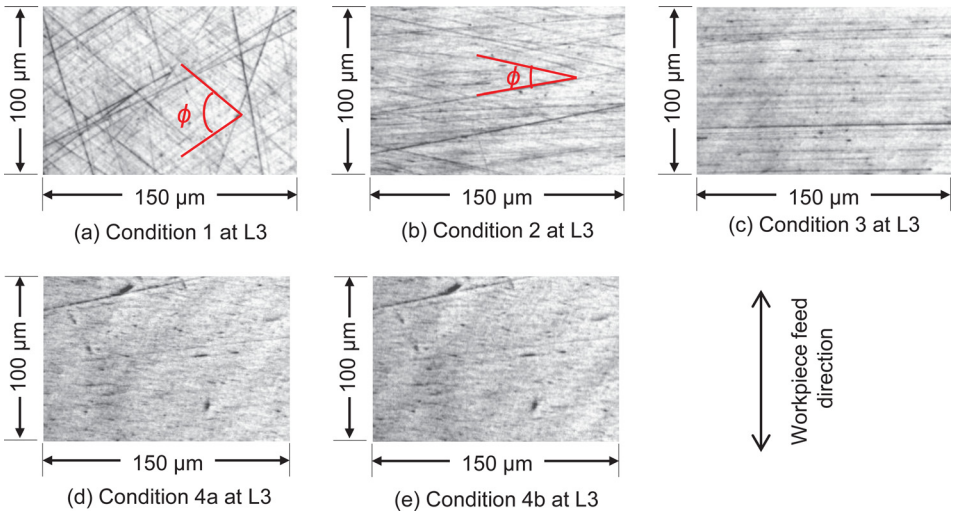

Fig. 6 Images of MAF-finished surfaces captured by an optical profilometer

Table 2 Cross-hatch angle

Finishing condition	Calculated angle (deg)	Measured angle (deg)
Condition 1	78.2	77.9 (±14.3)
Condition 2	18.5	20.7 (±5.2)
Condition 3	0.4	0 (±0)

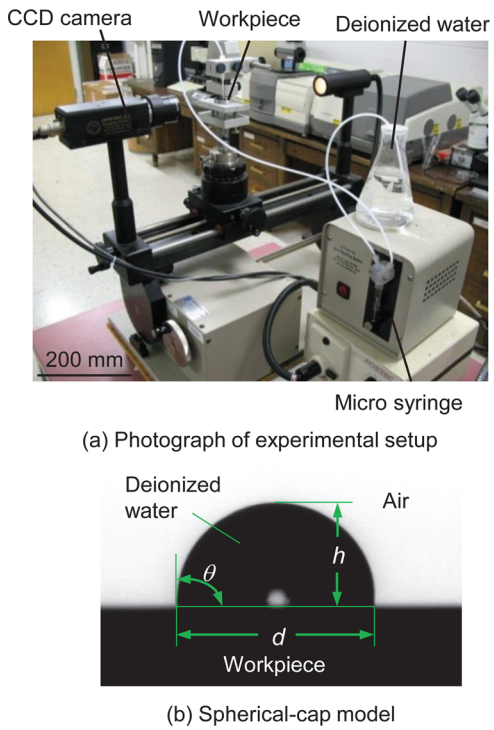

Fig. 7 Goniometer setup and contact angle θ

for each condition in Table 2 (standard deviations are reported in parentheses). The angle ϕ is also calculated as

$$\phi = 2(90^\circ - \Theta) \tag{6}$$

where Θ is the inclination angle in Eq. (5). The calculated values are also shown in Table 2.

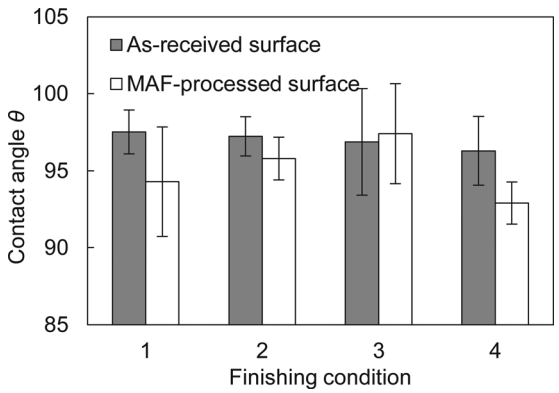

Fig. 8 Contact angle as a function of finishing conditions

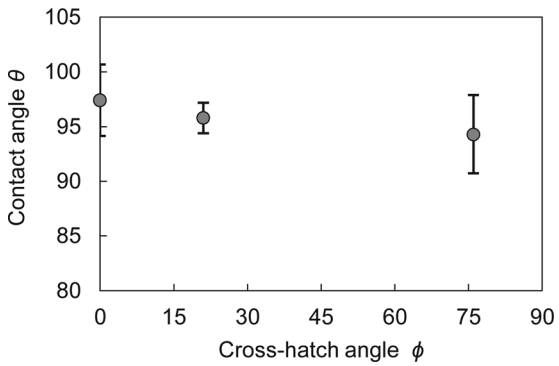

Fig. 9 Changes in contact angle with cross-hatch angles

The cross-hatch angles at the location corresponding to the pole-tip edge in conditions 1, 2, and 3 were calculated as 78.2 deg, 18.5 deg, and 0.4 deg. The measured angles are 77.9 deg, 20.7 deg, and 0 deg, respectively. The smaller workpiece feed rate resulted in a larger cross-hatch angle. It is also noted that the calculated and measured values agreed well, demonstrating that the suspended magnetic particles accurately follow the pole-tip rotational motion. The major differences between conditions 1–3 are the relationships between the workpiece feed rate and pole-tip rotational speed. In other words, the relationship between linear and rotational motion was varied. The ratios $R\omega/v_f$ are 1.23, 6.15, and 307.3 in conditions 1, 2, and 3, respectively, and the increased

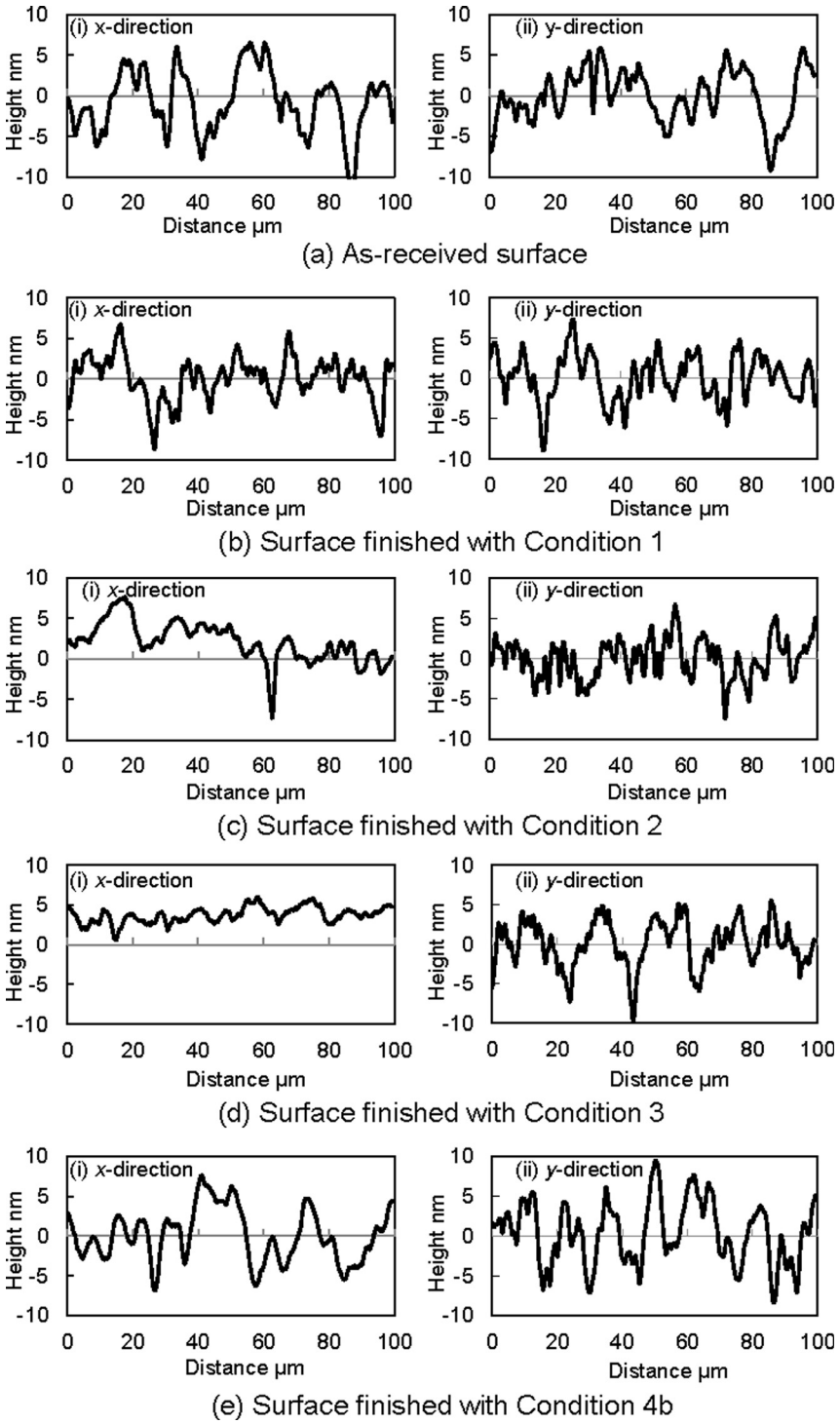

Fig. 10 Surface roughness profiles in *x*- and *y*-directions

ratio produces a decreased cross-hatch angle. The rotational motion dominates when the ratio is high, resulting in unidirectional cutting marks.

Condition 4 a produced a finished surface consisting of short, intermittent cutting marks using small magnetic particles. The small magnetic particles resulted in a smaller magnetic force acting on the particles and in turn the finishing force of the abrasive. The small magnetic force acting on the magnetic particles causes difficulties in overcoming the finishing friction and encourages relocation of the magnetic particles within the particle chains. This facilitates the production of shallow marks and leaves the deep scratches observed on the as-received surface. The finishing action in condition 4 b was performed in a weaker magnetic field due to a lower exciting current and removed the peaks while maintaining the lay.

Accordingly, the finishing experiments demonstrated that MAF can alter the surface lay while controlling the nanometer-scale surface roughness. The magnetic force (controlled by particle size and exciting current) influences the particle motion within the particle chains and alters the contact between the magnetic particles and target surface, which determine the length and depth of the cutting marks. With chains made of stiffly linked magnetic

particles, the surface lay is the result of the cycloidal motion of the particles, which is the result of the rotational motion of the pole tip and the linear motion of the workpiece. Using four different surface lays produced by MAF, the effects of lay on the contact angle of deionized water (i.e., the wettability) are studied in the following chapter.

6 Effect of Surface Pattern on Wettability

A contact-angle goniometer was used to measure the wettability of the workpieces. The experimental setup is shown in Fig. 7(*a*). The workpieces were cleaned with acetone and rinsed with ethanol prior to the measurement and set in front of a CCD camera. Two microliters of deionized water was deposited using a microsyringe, and the droplet shape was recorded and analyzed. As shown in Fig. 7(*b*), the droplet is hemispherical. The static contact angle θ is given as a function of the droplet height h and diameter of contact area d

$$\theta = 2 \cdot \tan^{-1}(2 \times h/d) \tag{7}$$

The contact-angle tests were conducted at each location (L1–L5 in Fig. 3(*a*)) for all workpieces. The contact angles were measured five times both parallel and normal to the workpiece feed direction. It has been reported that the droplet tends to spread along grooves on submicrometer scale surfaces, reducing the contact angle [33]. In other words, the contact-angle measurements could be influenced by the directionality of the lay. However, the effects of the measurement direction (either parallel or perpendicular to the workpiece feed direction) on the contact angle of the droplets were not detected in this study. The average of five contact angles measured at each location in the workpiece feed direction are shown as representatives.

Figure 8 shows the contact angles (before and after MAF) for each finishing condition. Figure 9 shows the relationship between the contact angle and cross-hatch angle for conditions 1–3. The as-received surface, consisting of random multidirectional cutting marks, had an average contact angle between 96 deg and 97 deg. After finishing, the contact angles of the MAF-processed surfaces (93 deg −97 deg) were smaller or nearly equal to those of the as-received surfaces. As shown in Figs. 10(*b*)–10(*d*), the differences in surface roughness profiles between the *x*- and *y*-directions are reduced with increasing cross-hatch angle. When the deionized water droplet is placed on the workpiece surface for the contact-angle measurement, the droplet tends to spread into the valleys of the surface asperities. The surface produced using condition 1, which has a large cross-hatch angle, encouraged the water droplet to flow outward in a radial fashion. In contrast, the surface from condition 3 consists of unidirectional cutting marks. The unidirectional lay could better constrain the spread of the water droplet in a direction perpendicular to the cutting marks (i.e., the *y*-direction), resulting in smaller changes in the droplet shape. As a result, the contact angles decreased with increasing cross-hatch angle. Condition 4 produced short, intermittent cutting marks. As shown in Fig. 10(*e*), the roughness profiles in the *x*- and *y*-directions are similar, although the peak-to-peak distances are slightly different. This might have facilitated the spread of the droplet in a radial fashion, resulting in the smallest contact angle.

Considering that the workpieces have similar surface roughness S_a and S_z, and the MAF process removes material without altering the workpiece's material properties, the only observable change to the workpiece is the surface lay. As such, these results show that wettability (i.e., contact angle) is a function of surface lay (in addition to the effect of surface roughness15–1733. Specifically, the results show that the contact angle decreases with decreasing directionality of the cutting marks.

7 Conclusions

The main findings from this paper can be summarized as follows:

(1) This paper demonstrated the feasibility of MAF to alter surface lay—from strongly directional surface to an isotropic surface—while controlling the nanometer-scale surface roughness by changing the magnetic force acting on the particles (using parameters such as particle size and magnetic field intensity) and the particle motion.
(2) Using four different surface lays produced by MAF, it was shown that the contact angle (i.e., wettability) is a function of surface lay on the nanometer-scale surface.
(3) Surfaces with unidirectional cutting marks exhibit the least wettability, and increasing the cross-hatch angle in the MAF-produced surfaces increases the wettability. Surfaces consisting of short, intermittent cutting marks with less directionality are the most wettable by deionized water.

Further research is essential to understand the fine details of the MAF-processed surface on freeform components (e.g., knee prostheses) and to clarify the effects of the surface lay on the wettability and other tribological properties. The study of MAF on freeform surfaces and the local control of the surface lay with nanometer-scale roughness should be included in further studies.

Acknowledgment

This work was supported by the National Science Foundation (Grant No. CMMI-0855381). The authors gratefully acknowledge the 2012 American Society of Mechanical Engineers Elisabeth M. and Winchell M. Parsons Scholarship. The authors also would like to thank James C. Wilkes and J. Whittaker Bullard for their interest in this work and Exactech, Inc., for their support in the workpiece preparation.

References

[1] Kulawiec, A., Kordonski, W., and Gorodkin, S., 2012, "New Approaches to MRF in Optical Fabrication and Testing," Imaging Applied Optics Technical Digest (online), Paper No. OM3D.3.
[2] Tricard, M., Kordonski, W. I., and Shorey, A. B., 2006, "Magnetorheological Jet Finishing of Conformal, Freeform and Steep Concave Optics," Ann. CIRP, **55**(1), pp. 309–312.
[3] Kordonski, W. I., and Golini, D., 1999, "Fundamentals of Magnetorheological Fluid Utilization in High Precision Finishing," J. Intell. Mater. Syst. Struct., **10**, pp. 683–389.
[4] Harris, D., 2011, "History of Magnetorheological Finishing," Proc. SPIE, pp. 1–22.
[5] Walker, D., Beaucamp, A., Dunn, C., Freeman, R., Marek, A., McCavana, G., Morton, R., and Riley, D., 2004, *First Results on Free-Form Polishing Using the Precessions Process*, Proc. ASPE Winter Conference: Freeform Optics, Design, Fabrication, Metrology, Assembly.
[6] Beaucamp, A., Matsumoto, A., and Namba, Y., 2010, "Ultra-Precision Fluid Jet and Bonnet Polishing for Next Generation Hard X-ray Telescope Application," Proc. ASPE, pp. 3184–1.
[7] Zeng, S., and Blunt, L., 2014, "Experimental Investigation and Analytical Modelling of the Effects of Process Parameters on Material Removal Rate for Bonnet Polishing of Cobalt Chrome Alloy," Precis. Eng., **38**, pp. 348–355.
[8] Cheung, C. F., Li, H. F., Lee, W. B., To, S., and Kong, L. B., 2007, "An Integrated Form Characterization Method for Measuring Ultra-Precision Freeform Surfaces," Int. J. Mach. Tools Manuf., **47**, pp. 81–91.
[9] Zeng, S., Blunt, L., and Jiang, X., 2012, "Material Removal Investigation in Bonnet Polishing of CoCr Alloy," Proceedings of The Queen's Diamond Jubilee Computing and Engineering Annual Researcher's Conference, pp. 25–30.
[10] Jain, V. K., and Sidpara, A., 2012, "Nanofinishing of Freeform Surfaces of Prosthetic Knee Joint Implant," Proc. Inst. Mech. Eng., Part B, J. Eng. Manuf., **226**(11), pp. 1833–1846.
[11] Fisher, J., Dowson, D., Hamdzah, H., and Lee, H. L., 1994, "The Effect of Sliding Velocity on the Friction and Wear of UHMWPE for Use in Total Artificial Joints," Wear, **175**(1-2), pp. 219–225.
[12] Ingham, E., and Fisher, J., 2005, "The Role of Macrophages in Osteolysis of Total Joint Replacement," Biomaterials, **26**(11), pp. 1271–1286.
[13] Borruto, A., Marrelli, L., and Palma, F., 2005, "The Difference of Material Wettability as Critical Factor in the Choice of a Tribological Prosthetic Coupling Without Debris Release," Tribol. Lett., **20**(1), pp. 1–10.
[14] Borruto, A., Crivellone, G., and Marani, F., 1998, "Influence of Surface Wettability on Friction and Wear Tests," Wear, **222**, pp. 57–65.
[15] Wenzel, R. N., 1936, "Resistance of Solid Surfaces to Wetting by Water," Ind. Eng. Chem., **28**, pp. 988–994.
[16] Cassie, A. B. D., and Baxter, S., 1944, "Wettability of Porous Surfaces," Trans. Faraday Soc., **40**, pp. 546–551.
[17] Kubiak, K. J., Wilson, M. C. T., Mathia, T. G., Carval Ph., 2011, "Wettability Versus Roughness of Engineering Surfaces," Wear, **271**, pp. 523–528.

[18] Encinas, N., Pantoja, M., Abenojar, J., and Martinez, M. A., 2010, "Control of Wettability of Polymers by Surface Roughness Modification," J. Adhes. Sci. Technol., **24**, pp. 1869–1883.
[19] Bhattacharya, S., Datta, A., Berg, J., and Gangopadhyay, S., 2005, "Studies on Surface Wettability of Poly(Dimethyl) Siloxane (PDMS) and Glass Under Oxygen-Plasma Treatment and Correlation With Bond Strength," J. Microelectromech. Syst., **14**(3), pp. 590–597.
[20] Chen, Y., Duh, J., and Chiou, B., 2000, "The Effect of Substrate Surface Roughness on the Wettability of Sn-Bi Solders," J. Mater. Sci.: Mater. Electron., **11**, pp. 279–283.
[21] Hallab, N., Bundy, K., O'Connor, K., Moses, R., and Jacobs, J., 2001, "Evaluation of Metallic and Polymeric Biomaterial Surface Energy and Surface Roughness Characteristics for Directed Cell Adhesion," Tissue Eng., **7**(1), pp. 55–71.
[22] Singh, R., Melkote, S., and Hashimoto, F., 2005, "Frictional Response of Precision Finished Surfaces in Pure Sliding," Wear, **258**, pp. 1500–1509.
[23] Malshe, A., Rajurkar, K., Samant, A., Hansen, H. N., Bapat, S., and Jiang, W., 2013, "Bioinspired Functional Surfaces for Advanced Applications," CIRP Ann. - Manuf. Technol., **62**(2), pp. 607–628.
[24] Mezghani, S., Demirci, I., Zahouani, H., and El Mansori, M., 2012, "The Effect of Groove Texture Patterns on Piston-Ring Pack Friction," Precis. Eng., **36**, pp. 210–217.
[25] Patil, M. G., Chandra, K., and Misra, P. S., 2011, "Magnetic Abrasive Finishing—A Review," Adv. Mater. Res., **418-420**, pp. 1577–1581.
[26] Kim, J., and Noh, I., 2007, "Magnetic Polishing of Three Dimensional Die and Mold Surfaces," Int. J. Adv. Manuf. Technol., **33**(1), pp. 18–23.
[27] Ji, S. M., Xu, Y. M., Chen, G. D., and Jin, M. S., 2011, "Comparative Study of Magnetic Abrasive Finishing in Free-Form Surface Based on Different Polishing Head," Mater. Sci. Forum, **675-677**, pp. 593–596.
[28] Jain, V. K., Singh, D. K., and Raghuram, V., 2008, "Analysis of Performance of Pulsating Flexible Magnetic Abrasive Brush (PFMAB)," Mach. Sci. Technol., **12**(1), pp. 53–76.
[29] Yamaguchi, H., and Shinmura, T., 1999, "Study of the Surface Modification Resulting From an Internal Magnetic Abrasive Finishing Process," Wear, **225-229**, pp. 246–255.
[30] Sato, T., Yamaguchi, H., Shinmura, T., and Okazaki, T., 2007, "Study of Internal Magnetic Field Assisted Finishing for Copper Tubes With MRF (Magnetorheological Fluid)-Based Slurry," Key Eng. Mater., **329**, pp. 249–254.
[31] Shinmura, T., Takazawa, K., Hatano, E., and Matsunaga, M., 1990, "Study on Magnetic Abrasive Finishing," Ann. CIRP, **39**(1), pp. 325–328.
[32] Graziano, A., Ganguly, V., Bullard, J., Yamaguchi, H., and Schmitz, T., 2012, "Characteristics of Cobalt Chromium Alloy Surfaces Finished Using Magnetic Abrasive Finishing," Proceedings of the ASME 2012 International Manufacturing Science and Engineering Conference, pp. 1–8.
[33] Kubiak, K. J., Wilson, M. C. T., Mathia, T. G., and Carval, Ph., 2009, "Wettability versus Roughness of Engineering Surfaces," Proceedings of 12th International Conference on Metrology and Properties of Engineering Surfaces, pp. 1–5.